Structure Population in Thiol-Passivated Gold Nanoparticles

D. Zanchet,[†,‡] B. D. Hall,[§] and D. Ugarte[†]

Laboratório Nacional de Luz Síncrotron, C.P. 6192, 13084-971 Campinas SP, Brazil, Instituto de Física Gleb Wataghin, UNICAMP, C.P. 6165, 13083-970 Campinas SP, Brazil, and Measurement Standards Laboratory of New Zealand, P.O. Box 31-310, Lower Hutt, New Zealand

Received: May 11, 2000; In Final Form: August 24, 2000

Chemically synthesized nanoparticles can be regarded as building blocks for more complex systems. Hence, the characterization of their attributes is a key step toward controlling and tuning the properties of new nanocomposite materials. We present a structural characterization of thiol-capped gold nanoparticles as a function of size (2−4 nm) by X-ray diffraction (XRD). In addition to the fcc bulk structure, nanometric gold may present decahedral or icosahedral structures depending on particle size. To evaluate the structure evolution, we have applied Debye function analysis to the XRD profiles. The analysis reveals a high proportion of defective and complex structures in all samples, which may have become trapped by the growth conditions. Nevertheless, the fcc structure is more prominent with increasing diameter, indicating that thermodynamics also plays an important role in the average structure of this system. The results underline the importance of performing careful structural characterization of chemically synthesized nanoparticles, in particular, in systems such as gold, where several distinct and stable structures are known to have little difference in energy.

1. Introduction

Nanostructured systems are currently attracting a great deal of interest because they can be used to generate novel materials.[1] A complex interplay, of individual and collective properties of the nanometric phases, defines the global material attributes and it is expected that by controlling the nanophase parameters (e.g., size, structure, etc.) it will be possible to tune fundamental properties (i.e., chemical, electrical optical, magnetic, etc.).

One proposed strategy for producing nanostructured materials is what we call the "bottom-up" approach, where presynthesized nanometric units are used to build up a macroscopic material. Here, the production of well-defined nanoparticle (NP) samples is the essential first step, and presents a fundamental challenge to both basic science and NP technology. It will be important to exert control over various structural and morphological NP parameters. The first sample parameter to be tackled is the NP size distribution, where wet chemistry has shown remarkable success.[2−4] The second parameter is shape, which may have an important influence, for example, on magnetic properties, where spherical and elongated particles show different behavior.[5] The control of this parameter is being investigated at present by several groups, and important progress has already been obtained.[6,7] A last characteristic to be optimized is the distribution of structures within a NP sample. In particular, NPs may show unique atomic arrangements as a result of their small size. A well-known case is the appearance of noncrystallographic structures (multiple twinned particles, MTPs), such as decahedra (dec) and icosahedra (ico), in noble metal particles where the bulk atomic arrangement is a face centered cubic (fcc).[8,9]

The determination of size and shape distribution can be addressed by different techniques, well-suited to characterize particles of a few nanometers in diameter (e.g., small angle X-ray scattering, SAXS; transmission electron microscopy, TEM). TEM yields direct real space information, and it represents the method most widely applied for chemically synthesized NPs. However, to determine the internal atomic arrangement within the NPs, high resolution TEM (HRTEM) and X-ray diffraction (XRD) are most commonly used. Although HRTEM permits direct imaging of atomic positions, the image-contrast is strongly dependent on NP orientation,[10,11] making a reliable statistical characterization of a complex NP system rather difficult to perform.

In this work, we report on the structural characterization of colloidal thiol-capped gold NPs by XRD. In particular, we have studied the evolution of the MTP fraction as a function of particle size (2−4 nm) and have also analyzed the possible effects of the passivating layer. We have found that the gold NP samples are highly defective, and cannot be described by perfect model structures (either fcc, or MTPs); these results are corroborated by HRTEM.

2. Experimental Details

Thiol-passivated gold NPs have been synthesized with the Brust method,[12] where a gold precursor ($HAuCl_4$) is reduced with simultaneous passivation by thiol molecules. By using the same protocol, but changing the Au:S molar ratio, it is possible to modify the NP size distribution.[13] We have prepared three different samples using dodecanethiol molecules (DOD) with approximate Au:S molar ratio values: 1:2, 2:1, and 4:1 and the resultant mean diameters were 2.0, 3.2, and 4.1 nm, respectively (as measured by TEM, see Figure 1a−c).[14] The size distributions have approximately the same width (FWHM $\approx$ 1 nm) for all three systems. We have used the same procedure with a shorter chain as a capping agent, butanethiol (BUT), to produce a sample with a mean diameter of 3.2 nm and a size distribution width of $\approx$1.4 nm. In general, our BUT-passivated nanoparticle

* Corresponding author. Laboratório Nacional de Luz Síncrotron—LNLS, C. P. 6192, CEP: 13084-971, Campinas SP Brazil. Phone: +55 19 3287 4520. FAX: +55 19 3287 4632. E-mail: ugarte@lnls.br.

[†] Laboratório Nacional de Luz Síncrotron.

[‡] Instituto de Física Gleb Wataghin.

[§] Measurement Standards Laboratory of New Zealand.

10.1021/jp0017644 CCC: $19.00
Published on Web 11/01/2000

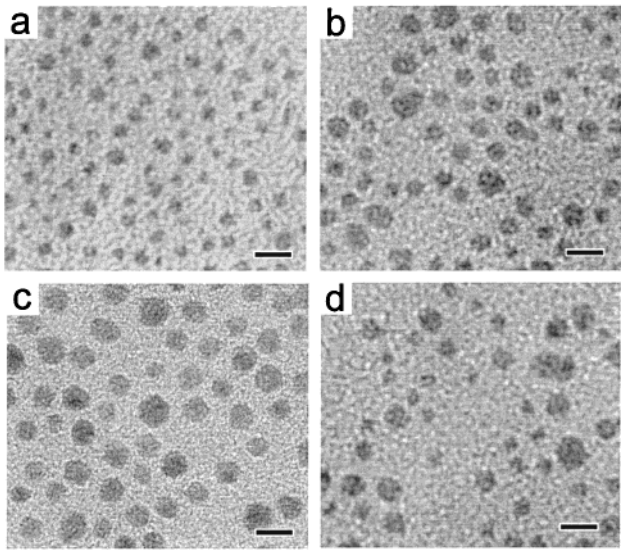

Figure 1. TEM images of thiol-passivated gold NPs (a) DOD 2.0 nm, (b) DOD 3.2 nm, (c) DOD 4.1 nm, (d) BUT 3.2 nm. The scale bar indicates 5 nm.

samples showed a broader size distribution (see Figure 1d), so we have limited our study of these to a single sample.

Powder XRD studies were realized on the XRD beam line at the Brazilian Synchrotron Light Facility (LNLS—Campinas, Brazil)[15] using 8.040 keV photons at room temperature. The incident X-ray beam was monochromatized by a Si (111) double crystal monochromator. As NP diffraction peaks are broad (FWHM $\approx$ 5 degrees for the [111] peak of 2 nm particles), we used a wide detection slit (2 mm) in front of the scintillation detector. The sample was prepared by slightly pressing the dried NP powder onto a glass substrate.

3. Data treatment

3.1 Analysis of XRD Measurements. The interpretation of diffraction measurements, performed on nanometer-sized particles, poses particular problems. Gold NPs in the 2−4 nm size range are a case in point. The finite size of these particles causes marked peak-broadening, as well as other size-related features. Also, there are potentially three distinct structure types (fcc, ico, dec) present, even coexisting, in these samples. Although each type has a distinct diffraction pattern, an experimental measurement can represent a convoluted mixture of structure types and sizes, and it is impossible to make a simple interpretation of such data. Furthermore, imperfectly formed particles may contain significant domains of well-defined structure.[16] Wide-angle XRD measurements are dominated by larger coherent regions of structure in a sample; hence, an analysis of XRD data actually yields information about the distribution of domain sizes, which is only indirectly related to the size distribution of the NPs.

To cope with this complexity, a computer-based analysis procedure has been used in this work. This procedure has been described in some detail recently,[17,18] including a test of its efficacy and a detailed discussion of the diffraction problem in NPs. While our procedure has been developed in the context of electron diffraction measurements,[19,20,21] a similar procedure, called Debye function analysis (DFA), has been used for X-ray measurements by Vogel and co-workers.[22,23] The two procedures differ in implementation detail, yet perform essentially the same analysis. Hence we take the liberty of referring to the analysis procedure used here as DFA, which may be familiar to readers of this journal.

DFA extracts information about the size distribution of structure domains by analyzing an experimental diffraction pattern. This is done by calculating individual diffraction patterns for a set of model particles, covering the range of sizes and structure types that may occur in the experiment, and finding the appropriate relative weightings of these profiles to match the experimental data. Global optimization is used to obtain the best match. To estimate variance in the results, due to measurement noise, we have made repeated analyses of the experimental data modified with an additional pseudo-random noise component. This produces a spread of fitted parameters that can be considered comparable to the variance arising from the original measurement noise, and allows us to quantify the uncertainty in our analysis (see ref 18 for more details).

DFA in this work used up to eighteen calculated diffraction profiles (three structure types, six models per type), covering particle sizes appropriate to the samples. In addition, an independently measured background profile was included and optimized to provide background subtraction. The raw weightings of model profiles, found by DFA, have been used to calculate the mean and standard deviation of the domain size distributions for each structure type.

To assess the uncertainty in these estimated values we use a simple Monte Carlo procedure. Ten data sets were constructed by adding the appropriate level of random (Poisson) noise fluctuations to the original observations. A separate DFA is then applied to each data set and the results used to calculate the average and standard deviations in the estimated values.[18] Let

$$d' = \frac{\sum_{i=1}^{m} n_i d_i}{\sum_{i=1}^{m} n_i} \tag{1}$$

be the average diameter calculated from a single application of DFA, using m calculated profiles, d_i is the diameter of the ith model and n_i is the weighting parameter for that profile, optimized by DFA. The statistic d_{av} is the average value of d' from 10 successive DFA applications. Similarly, let

$$d_v' = \frac{\sum_{i=1}^{m} n_i v_i d_i}{\sum_{i=1}^{m} n_i v_i} \tag{2}$$

where v_i represents the volume of the ith model, then d_{av} (the average of 10 successive DFA applications) is the volume-weighted average diameter. (Note that it is the volume weighted distribution that represents the relative intensities in diffraction)

3.2. Estimate of Particle Size from XRD Data. A Fourier inversion method has been applied to the XRD data to estimate the size of NPs, and corroborate TEM observations. Traditionally, the so-called Scherrer formula would be applied directly to a single diffraction peak in XRD data; for small crystals, the half-width of the peak is simply related to the characteristic particle size.[24] Unfortunately, the Scherrer formula cannot be applied to either dec of ico nanoparticles, nor is it very reliable in ultra-small fcc nanoparticles where overlapping peaks are difficult to account for. Fourier inversion provides a robust alternative that makes no assumptions regarding particle structure.

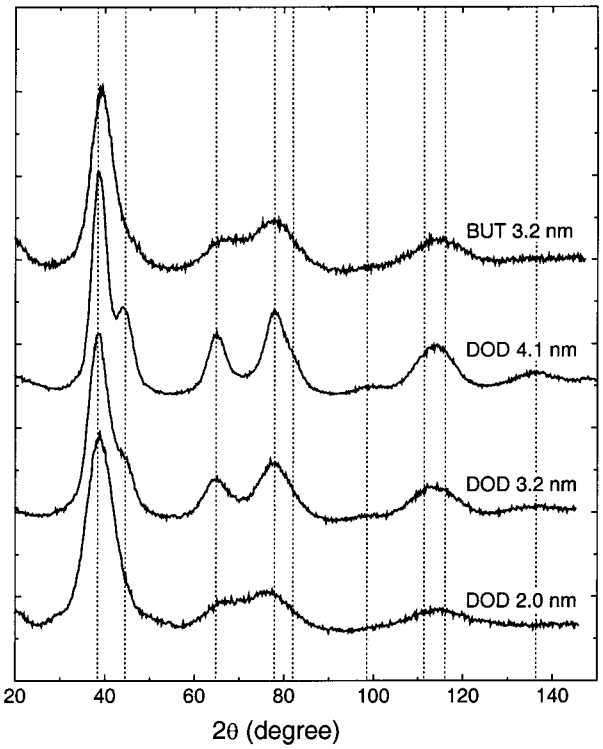

Figure 2. Powder X-ray diffraction patterns of three DOD-passivated NPs (lower three curves), and BUT-passivated NPs (upper curve). The positions of bulk gold Bragg peaks are indicated with dashed vertical lines for reference.

It is possible to estimate the sample distribution of interatomic distances by taking a Fourier transform of the diffracted intensity.[24] Fourier inversion is usually applied to data which extend to high values of scattering parameter, where diffracted intensity is very weak. However, in this study the upper limit of the scattering parameter, determined by the wavelength of the incident X-rays, is rather severe. As a consequence, the spatial resolution of the transformed data reciprocal is not sufficient to obtain reliable information about the internal particle structures. Nevertheless, Fourier inversion can make a good estimate of the characteristic size of particles in a sample.

The inversion procedure uses the fact the distribution of interatomic distances is bounded above in NPs, which are of finite size. This upper limit can identified by visual inspection of the transformed data with quite acceptable accuracy (for more details see ref 25). An iterative procedure is implemented: initially, a normalization factor representing the incident intensity− times the number of scattering atoms is estimated and used to rescale the experimental data before Fourier transformation. This factor is then varied between successive iterations, until a satisfactory solution is obtained. The results are fairly insensitive to the value of normalization factor and the procedure has provided results in this study that are consistent with TEM observations (uncertainty $\sim \pm 0.2$ nm).

4. Results and Discussion

Figure 2 displays the powder diffraction patterns of our four NP samples. The broad peaks in these patterns are roughly aligned with the positions of Bragg diffraction from the bulk gold atomic planes (dashed lines). For the three DOD-passivated NP samples (lower curves in Figure 2), a quick inspection of the diffraction profiles reveals broadening of the diffraction features, as the mean particle size decreases, and no significant change in peak positions. It would be at this point too simplistic to attribute the pattern differences only to size-broadening effects (see section 3.1), since gold NPs may assume different structures: detailed DFA analysis is necessary to extract structural information. The recent work of Vogel et al.[26] represents an illustrating example of the application of this approach to gold.

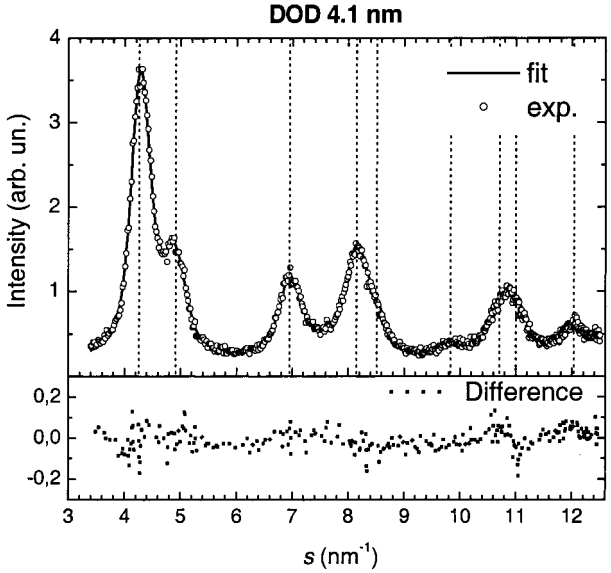

Figure 3. Results of the DFA analysis applied to the DOD 4.1 nm sample. The upper window shows the superposition of experimental (dotted line) and DFA curves (solid line). The lower window shows the simple difference between the two curves.

TABLE 1: DFA Analysis of the DOD Passivated Gold NPs: The Statistics Report the Means and Standard Deviations of the Structure-Specific Domain Size Distributions Obtained by DFA[a]

structure	d_{av} (nm) number	std	d_{av} (nm) vol.	std	% number	% vol
			2.0 nm DOD-Capped			
fcc	-	-	-	-	-	-
ico	1.2(−)	0.2(−)	1.3(−)	0.4(0.1)	48(1)	45(1)
dec	1.3(−)	0.4(−)	1.6(−)	0.6(0.1)	52(1)	55(1)
total	1.2(−)	0.3(−)	1.5(−)	1.3(−)		
			3.2 nm DOD-Capped			
fcc	2.7(0.1)	0.3(0.1)	2.9(0.1)	0.3(0.2)	5(1)	13(1)
ico	1.8(0.2)	0.4(0.2)	2.0(0.1)	0.2(0.1)	17(4)	18(1)
dec	1.7(0.1)	0.5(−)	2.2(−)	0.5(0.2)	78(4)	69(2)
total	1.8(−)	0.6(−)	2.3(−)	1.3(0.1)		
			4.1 nm DOD-Capped			
fcc	3.2(0.2)	0.4(0.2)	3.3(0.1)	0.6(0.3)	14(2)	22(1)
ico	2.5(0.1)	0.2(0.1)	2.5(0.1)	0.4(0.4)	11(3)	9(2)
dec	2.5(−)	0.7(−)	3.1(0.1)	1.0(0.1)	75(3)	69(2)
total	2.6(−)	0.6(−)	3.1(−)	1.4(0.2)		

[a] The "total" row lists means and standard deviations of the combined domain size distribution, irrespective of structure type. Also reported are the percentages, by number and by volume, of each structure type. The uncertainty in all estimated values is shown in parentheses. These were evaluated using a Monte Carlo technique (section 3.1). All numbers have been rounded to the nearest integer (if this happens to be zero, a "−" has been entered).

In Figure 3, we show the DFA best-fit profile for the DOD-capped 4.1 nm sample superimposed on the experimental diffraction pattern. Also we display the difference between the two curves in the lower window, which shows that DFA can account for the experimental features. Similar quality fits were obtained for the other NP samples analyzed in this work. Table 1 records quantitative information on the DOD samples for the domain size distribution of each structural type (fcc, dec, and

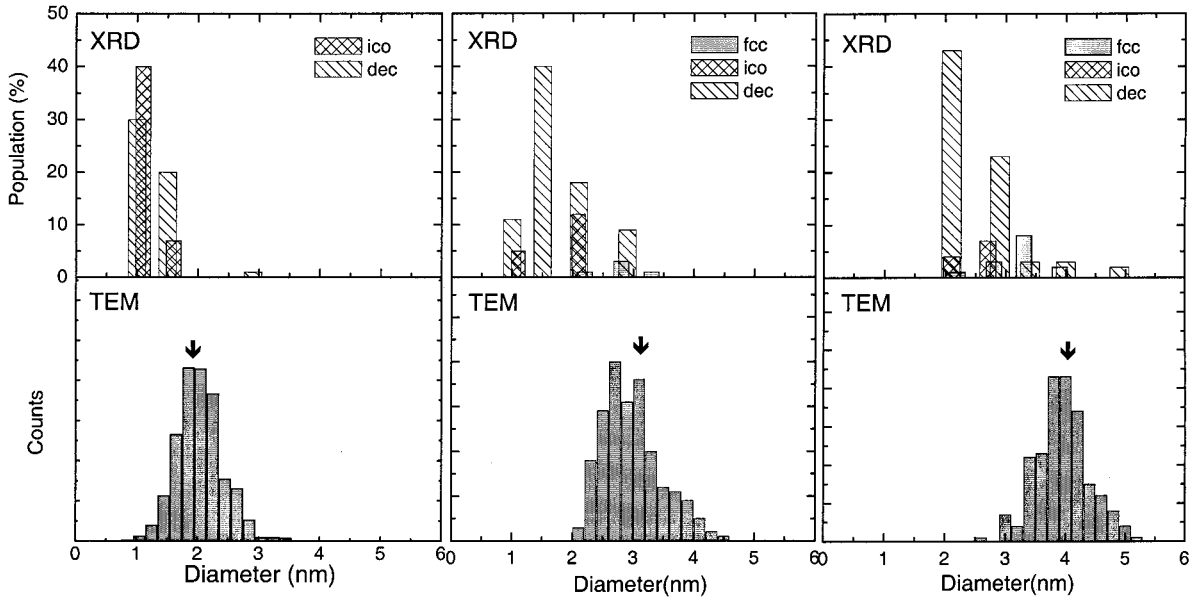

Figure 4. Comparison of the size distribution derived for the DOD samples. The upper windows show DFA results for the three structural models used in the analysis (fcc, dec, ico). The lower window displays the TEM measured diameter distribution. (a) 2.0 nm, (b) 3.2 nm, (c) 4.1 nm samples.

ico), deduced from the results of the DFA analysis, and using the expressions in section 3.1. For each sample, the table shows the mean size, for each structure type, as well as the standard deviation of the corresponding distribution, and the percentage of the structure type in the analysis. These statistics are reported for the domain size distributions as well as the domain size distributions weighted by NP volume.

The first noticeable result in Table 1 is the high proportion of MTPs found in all samples. For the 2.0 nm sample, decahedral and icosahedral structures are found in roughly equal quantities while no fcc particles were detected. An fcc population is observed for the 3.2 nm particles, and becomes more important for the 4.1 nm sample. In both these samples, the increasing importance of the fcc population is associated with a decrease in ico numbers, this is particularly significant for the 4.1 nm system. For all three DOD-capped samples, decahedral particles form a majority.

A second important result is the difference between the mean diameters derived from the diffraction pattern analysis and those derived from TEM observations; in all cases, DFA-derived diameters are smaller. This observation can be analyzed by comparing the DFA domain size distribution results with the particle size distributions obtained by TEM, shown in Figure 4. For example, looking to the 4.1 nm sample (Figure 4c), the majority of MTPs and a significant percentage of fcc are in the small size region ([1−2.5] nm); however, it is also important to note that there are decahedral and fcc domains with sizes very close to the TEM diameters (∼3−4 nm). This strongly suggests the existence of single-structure (fcc and dec) particles in the sample, mixed in with imperfect NPs. Similar structural tendencies were observed for the 3.2 nm particles.

There are, nevertheless, significant variations between the size distributions derived from TEM and DFA. This is not surprising if one considers that the TEM observations resolve the external particle boundary; DFA, on the other hand, is based on the information contained in the limited angular range of the XRD data and is directly related to the interatomic arrangement.[18] When particles are perfect monodomain crystal structures, DFA should deduce a mean diameter in agreement with TEM observations (the volume-weighted mean will be a better estimator). However, for imperfect structures, DFA sees the diffraction pattern as a mixture, dominated by the largest crystalline domains within the particles: obviously these will be smaller than the particles themselves.

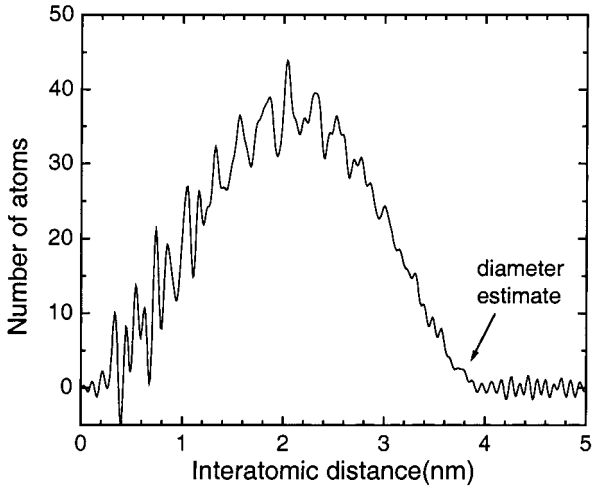

Figure 5. Interatomic distance distribution in the 4.1 nm sample, obtained by the Fourier inversion of the XRD pattern. An arrow indicates the estimated average mean diameter. This figure has been visually enhanced for the reader by assuming a spherical particle form and analytically recreating the small angle part of the diffraction pattern, which was not measured. This restores the "baseline" of the interatomic distribution. It does not impact on the estimate of characteristic particle size.

In this study, we have cross-checked the consistency of the XRD diffraction data with the observations obtained from TEM on the same samples. The Fourier inversion method, described in section 3.2, has been applied to the XRD data from each sample and yielded results in agreement with the corresponding TEM values, confirming the coherence of XRD and TEM data. An example is shown in Figure 5 for the DOD-capped 4.1 nm sample.

As a result, DFA analysis of the thiol-capped gold NPs reveals that the structural domains (mainly MTPs) are actually smaller than particle sizes. This can be explained in two ways. First, our particles could be complex (i.e., not perfectly formed

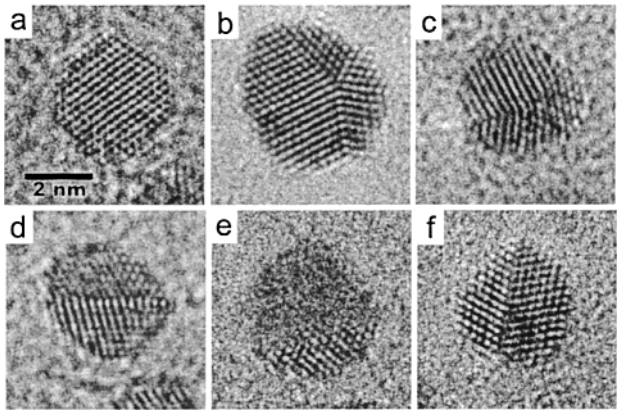

Figure 6. Typical HRTEM micrographs of NPs from the DOD-capped 4.1 nm sample. (a) fcc clusters, (b and c) decahedra, (d−f) multidomain particles.

polyhedral clusters) and perhaps composite (e.g., a small fcc domain joined to a dec/ico domain) structures. In the case of electron diffraction studies of Argon clusters, for example van de Waal[27] has proposed a polydecahedral model, formed by two decahedral nuclei and two fcc domains, to describe the experimental profiles. Our analysis would interpret this kind of structure as discrete decahedral and fcc domains, not a single particle. Although we cannot claim the existence of such an structure in our samples, this is an interesting example of the kind of composite nanoparticles that might indeed occur. Second, imperfections and defects in fcc particles show up as additional, small MTPs in the DFA. This DFA side effect occurs because, as explained in the section 3, a limited number of models are used to perform the DFA optimization procedure: the inclusion of very small model profiles can improve the match to faulted and complicated structures. DFA analysis of gold nanoparticles produced by the induced coalescence of smaller clusters has shown similar results, which has been interpreted as significant microstrain between the different domains.[26] In the present study, particles have been prepared by a "softer" procedure (i.e., wet chemical synthesis) and one would not expect such large micro-strains, because aggregation of preformed domains is unlikely to occur.

XRD measurements include diffraction data from many particles in a sample. It is essential to compare the results of an analysis of XRD data with other methods, such as HRTEM, so that image individual particles can be identified and that the internal atomic arrangements can be resolved. Figure 6 shows images typical of the DOD-capped 4.1 nm sample, where it is possible to identify different structural patterns. Figure 6a−c show particles that can be associated with single-structure particles: (a) fcc observed along the [110] direction and (b) and (c) decahedral particles oriented along the 5-fold axis. In contrast, Figure 6d−f show particles with defects (e.g., twins, or multidomain) for which a precise determination of their structure is not straightforward. In particular, Figure 6e resolves the atomic arrangement of only half of the particle, indicating that there are at least two domains with different orientations. This particle could consist of two fcc domains that are joined coherently or incoherently. At this point, one must consider the existence of twinned fcc particles in the samples; in fact, Cleveland et al.[28] have predicted an insignificant energy difference between twinned fcc and pure fcc particles in this size range. Surprisingly, however, when twinned fcc models were included in our DFA analysis, they neither improved the fit to the experimental XRD pattern nor appeared as a significant structural component. Hence they have not been included in our final analysis. HRTEM images strongly support the results obtained by DFA, indicating the existence of single-structure (fcc and dec) and faulted/complex forms. We must emphasize, however, that electron microscopy can only identify a small number of particles**,** which happen to be in a favorable orientation for imaging. DFA, on the other hand, yields statistically reliable estimates from a much larger sample and hence allows us to exclude twinned particles from the set of possible structures.

Theoretical predictions for the evolution of NP structure with size indicate that there should be a trend: starting with the icosahedron, at very small sizes ($\sim$<1 nm), then the truncated decahedron and finally to the bulk structure (fcc) at large sizes.[16] A recent study by Cleveland et al.[28] reported that the most competitive structures in the 1−3 nm range are the Marks decahedron and truncated-octahedron variants. Nevertheless, calculations of the energetic ordering among competing structures are very sensitive to faceting and surface environment: comparisons between theory and experiments are not expected to be straightforward.

The results obtained in this study do show something of the predicted tendency in size for gold NPs (ico → dec → fcc, for increasing size). First, mean icosahedral domain sizes are consistently smaller than the characteristic particle size, indicating an absence of single-particle icosahedra. Second, monodomain fcc and decahedral structures were found in larger particles (>3 nm − no fcc particles were detected in the 2.0 nm sample). Furthermore, the decahedral-domain mean diameter is smaller than fcc, suggesting that the later are more stable in bigger particles (bulk limit). Finally, the proportion of the fcc population in the sample is greater in the 4.1 nm sample, than that in the 3.2 nm one, as would be expected.[16]

This agreement with predictions for free gold clusters, where no passivant effect is taken into account, is rather remarkable. On the other hand, the existence of a large number of defective and complex particles cannot be explained thermodynamically.[16] This situation is particularly critical for the 2 nm particles with only about 200 atoms, however the larger particles (3.2, 4.1 nm) contain several thousand atoms and defective structures could be expected. It is important to realize that, in the chemical synthesis, thiol-capped gold particles are formed in a low-temperature reaction, where the kinetics are likely to have a strong influence on metastable structures that form. This is an important issue in the field of NP chemical synthesis, and has been addressed only recently.[29] For example, a new phase of cobalt has been reported in chemically synthesized NPs, which completely transforms to the expected fcc phase under heating.[30] This result underlines the critical role of the growth conditions in crystals formed by low-temperature wet-chemistry procedures.

For thiol-capped gold NPs, the reaction conditions are known to affect the width of the size distribution (temperature, reducing agent addition, etc.).[31] This supports the idea that the kinetic of the process is important, and consequently it may also influence the distribution of structures in the sample. Nevertheless, the mean particle size is mainly determined by the thiol/gold ratio, which suggests a process close to thermodynamic equilibrium. Generalization of the results obtained from one batch of samples must be treated with care, since procedure details may modify the synthesis kinetic influencing significantly the generated NPs.

The possible influence of different thiol molecules at the surface of the particles has been studied using a gold NP sample passivated by butanethiol. The TEM size distribution for this sample showed a mean diameter of 3.2 nm and a width ($\sim$1.4 nm) which is slightly larger than the DOD-capped particles of

TABLE 2: DFA Analysis of the BUT-Passivated Gold NPs[a]

structure	d_{av} (nm) number	std	d_{av} (nm) vol	std	% number	% vol
			3.2 nm BUT-Capped			
fcc	–	–	–	–	–	–
ico	1.6(0.1)	0.3(0.1)	1.7(−)	0.3(0.2)	43(1)	41(4)
dec	1.7(0.1)	0.3(0.1)	1.9(0.1)	0.4(0.3)	57(5)	59(4)
total	1.6(0.1)	0.4(−)	1.9(−)	0.1(−)		

[a] See also title and footnote for Table 1.

same average size. This is a first indication that particle formation may be influenced by the passivant type.

The diffraction pattern from this sample, shown in Figure 2, has quite a different form compared to the equivalent DOD-passivated NP sample in Figure 1. DFA applied to this measurement found that only MTPs are present in the sample (see Table 2), in sharp contrast to DOD 3.2 nm, where a significant percentage (13 vol %) of fcc particles were detected. This strongly suggests that the distribution of sample structure types can be influenced by the choice of passivant used in the synthesis. However, it is not possible to conclude from these data alone whether these structural changes are due to thermodynamic surface-energy effects, or to a modification of the growth kinetics. We note that, as mentioned above, inclusion of twinned fcc structures in the DFA did not enhance the quality of the fit, or lift the negligible fraction of fcc structures (twinned or not).

5. Conclusions

The structure of thiol-passivated gold NPs, synthesized by wet chemistry methods, has been studied in detail using XRD and HRTEM measurements. It has been possible to determine the domain size-distributions of fcc cuboctahedra, decahedra, and icosahedra in NP samples by careful analysis of XRD patterns. We have been able to analyze the sample-mean size dependence of these distributions in the 2−4 nm range.

For dodecanethiol passivated particles, we found a high proportion of defective and complex structures, which were probably trapped by the kinetics of the growth conditions. Despite this, we have been able to identify an underlying structural tendency, correlated to mean particle diameter, which follows the expected theoretical tendency for free gold clusters (from ico to dec to fcc, with increasing particle size), suggesting that thermodynamics still plays an important role in determining the general structure of this system.

We have looked for a possible effect on the particle structure due to different passivants and found that butanethiol induces the formation of more multiple-twinned particles than dodecanethiol. Although further studies should be carried out, our results suggest that passivant properties could be exploited to modify and, maybe manipulate, the structure distribution in chemically synthesized samples.

Our results underline the importance of performing careful structural characterization of chemically synthesized NPs, in particular, in systems such as gold, where several distinct structures types are known to be very close in energy. Many issues still need to be addressed, to allow a full understanding of the structure dependence on synthesis conditions, however, it is clear that methods which can provide detailed structural information, like DFA and HRTEM, represent essential tools for characterization of NP systems.

Acknowledgment. The authors acknowledge the invaluable help of the LNLS staff. Electron microscopy studies were performed at the LME/LNLS-Campinas (JEM 3010 ARP), CIME-EPFL-Lausanne (Philips EM430T), and Centro. Mic. Eletrônica-UFRGS-Porto Alegre (JEM 2010 ARP). We thank financial support from CNPq and FAPESP (Proc. 96/12550-9, 97/04236-4). B.D.H. gratefully acknowledges travel assistance from the Royal Society of New Zealand (00-BRAP-11-HALL), and financial support under NSOF-N089134.

References and Notes

(1) Alivisatos, A. P.; Barbara, P. F.; Castleman, A. W.; Chang, J.; Dixon, D. A.; Klein, M. L.; McLendon, G. L.; Miller, J. S.; Ratner, M. A. *Adv. Mater.* **1998**, *10*, 1297 and references therein.

(2) Peng, X.; Wickham, J.; Alivisatos, A. P. J. *Am. Chem. Soc.* **1998**, *120*, 5343.

(3) Alvarez, M. M.; Khoury, J. T.; Schaaff, T. G.; Shbnafigullin, M.; Vezmar, I.; Whetten, R. L. *J. Phys. Chem. B.* **1997**, *101*, 3706.

(4) Sun, S. H.; Murray, C. B.; Weller, D.; Folks, L.; Moser, A. *Science* **2000**, *287*, 1989.

(5) Bucher, J. P.; Douglas, D. C.; Blomfield, L. A. *Phys. Rev. Lett.* **1991**, *66*, 3052.

(6) Lisiecki, I.; Filankembo, A.; Sack-Kongehl, H.; Weiss, K.; Pileni, M. P.; Urban, J. *Phys. Rev. B* **2000**, *61*, 4968.

(7) Peng, X.; Manna, L.; Yang, W.; Wickham, J.; Scher, E.; Kadavanich, A.; Alivisatos, A. P. *Nature* **2000**, *404*, 59.

(8) Ino, S. *J. Phys. Soc. Jpn.* **1969**, *26*, 1559.

(9) Ino, S. *J. Phys. Soc. Jpn.* **1969**, *27*, 941.

(10) Flüeli, M. Observation des Structures Anormales de Petites Particules d′Or et d′Argent par Microscopie Életronique à Haute Résolution et Diffraction d′Électrons par un Jet d′Agrégats d′Argent, Thèse No 769, Ecole Polytechnique Fédérale de Lausanne, Switzerland, 1989.

(11) Malm, J.-O.; O′Keefe, M. A. *Ultramicroscopy* **1997**, *68*, 13.

(12) Brust, M.; Walker, M.; Bethell, D.; Schiffrin, D. J.; Whyman, R. *J. Chem. Soc., Chem. Commun.* **1994**, 801.

(13) Brust, M.; Bethell, D.; Schiffrin, D. J.; Kiely, C. J. *Adv. Mater.* **1995**, *7*, 795.

(14) Zanchet, D.; Tolentino, H.; Martins Alves. M. C.; Alves. O. L.; Ugarte, D. *Chem. Phys. Lett.* **2000**, *323*, 167.

(15) Cusatis, C.; Franco, M. K.; Kakuno, E.; Giles, C.; Morelhao, S.; Mello, V.; Mazzaro, I. *J. Synchrotron Rad.* **1998**, *5*, 491.

(16) Marks, L. D. *Rep. Prog. Phys.* **1994**, *57*, 603.

(17) Zanchet, D.; Hall, B. D.; Ugarte, D. In *Characterization of Nanophase Materials*; Wang, Z. L., Ed.; VCH−Wiley: Weinheim, 1999.

(18) Hall, B. D. *J. Appl. Phys.* **2000**, *87*, 1666.

(19) Hall, B. D.; Flüeli, M.; Monot, R.; Borel, J.-P. *Z. Phys. D* **1989**, *12*, 97.

(20) Hall, B. D.; Flüeli, M.; Monot, R.; Borel, J.-P.; *Phys. Rev. B* **1991**, *43*, 3906.

(21) Reinhard, D.; Hall, B. D.; Ugarte, D.; Monot, R. *Phys. Rev. B* **1997**, *55*, 7868.

(22) Gnutzmann, V.; Vogel, W. *J. Phys. Chem.* **1990**, *94*, 4991.

(23) Vogel, W.; Cunningham D. A. H.; Tanaka, K.; Haruta, M. *Catal. Lett.* **1996**, *40*, 175.

(24) Guinier, A. *X-ray Diffraction in Crystals, Imperfect Crystals, and Amorphous Bodies*; Dover: New York, 1994.

(25) Hall, B. D.; Zanchet, D.; Ugarte, D. J. *Appl. Crystallogr.* Accepted for publication.

(26) Vogel, W.; Bradley, J.; Vollmer, O.; Abraham, I. *J. Phys. Chem. B* **1998**, *102*, 10853.

(27) van de Waal, B. *Phys. Rev. Lett.* **1996**, *76*, 1083.

(28) Cleveland, C. L.; Landman, U.; Schaaff, T. G.; Shafigullin, M. N.; Stephens, P. W.; Whetten, R. L. *Phys. Rev. Lett.* **1997**, *79*, 1873.

(29) Sun, S.; Murray, C. B. *J. Appl. Phys.* **1999**, *85*, 4325.

(30) Dinega, D. P.; Bawendi, M. G. *Angew. Chem., Int. Ed.* **1999**, *38*, 1788.

(31) Hostetler, M. J.; Wingate, J. E.; Zhong, C. J.; Harris, J. E.; Vachet, R. W.; Clark, M. R.; Londono, J. D.; Green, S. J.; Stokes, J. J.; Wignall, G. D.; Glish, G. L.; Porter, M. D.; Evans, N. D.; Murray, R. W. *Langmuir* **1998**, *14*, 17.